



Conductivity Fluctuation and Some Parameters of High temperature Superconductor Polycrystalline $Y_1Ba_2Cu_3O_{7-\delta}$ doped with Silver Nanoparticles

Gholamabbas Shams¹  · Morteza Ranjbar²

Received: 2 January 2019 / Published online: 13 September 2019
© Sociedade Brasileira de Física 2019

Abstract

In this study, we report the effect of Ag nanoparticles doping on the dimensional fluctuations of superconducting order parameters, crystal structure, and some parameters of $Y_1Ba_2Cu_3O_{7-\delta} + x Ag$ ($x = 0.0, 0.06, 0.1, 0.3,$ and 0.6 wt%) polycrystalline ceramics. By increasing the content of Ag in YBCO matrix, X-ray diffraction (XRD) with the Rietveld refinement technique revealed that the crystal lattice parameters changed and the orthorhombicity decreased slightly. Also, the increase of Ag wt% caused a decrease of superconducting transition temperatures (T_c) which are determined from the standard four-probe method and dropped abruptly. Aslamazov–Larkin (AL) model was used to analyze excess conductivity fluctuation. Lawrence–Doniach (LD) temperature named T_{LD} which is responsible for the dimensional nature of fluctuation inside the grains is influenced by nano-silver combination in the compound. Crossover temperature from 2D to 3D (T_{LD}) decreased in the mean-field region as a resultant dominance of 3D region by increasing of Ag in YBCO matrix. The decrease in zero-resistance critical temperature ($T_{c\ zero}$), zero-temperature coherence length along the c -axis $\xi_c(0)$, and super layer length d values implies the degradation of inter-grain weak links, more disorder state of samples and unsettling of the mean free path for the charge carriers respectively with addition of silver nanoparticles. The calculations based on AL and LD model showed the highest anisotropy ($\gamma = 1.34681$) for the $x = 0.6$ sample. The size of the Ag ions, being larger compared to Cu ions, and the number of substitution sites affects the coupling between the CuO₂ planes and that results in higher anisotropy. Critical magnetic fields $B_{c1}(0)$, $B_{c2}(0)$, and critical current density $J_c(0)$ were indirectly calculated from the Ginzburg–Landau (GL) number and GL equations. By increasing the doping level of silver nanoparticle, these parameters were found to be higher in Ag-added YBCO samples compared to the pure Y123, meaning better intrinsic flux pinning properties of doped Y123. The silver nanoparticle inclusion reduces the grain size and increases the strength and hardness of the parent compound.

Keywords Conductivity fluctuation · YBCO · Ag nanoparticle · Critical parameters

1 Introduction

Accurate knowledge of the thermal and electrical properties of pure and doped YBCO high-temperature superconductor still remains one of the more interesting subjects in these materials. For improvement of superconducting properties

of YBCO composites, researchers have been extensively studied these materials with different impurities such as SnO₂, CeO₂, CoFe₂O₄, BaZrO₃, Al₂O₃, Au, Al, and Ag [1–7]. Some of these impurities with nanometer particles like Mn₃O₄, Co₃O₄, Cr₂O₃, NiO, and Ce improve the superconductivity of bulk YBCO composites [2, 8, 9]. However, according to literature, doping superconductors by nanometer particles is an important technique in order to represent an easily controlled, non-destructive, and efficient tool for improving the mechanical, structural, and superconducting properties of the doped compounds which may lead to unexpected changes in the behavior of the superconductor [5]. A specific impurity such as Ag-doping enhances the inter-granular couplings of YBCO through grain alignment,

✉ Gholamabbas Shams
shams@iaushiraz.ac.ir

¹ Department of Physics, Shiraz Branch, Islamic Azad University, Shiraz, Iran

² Young Researchers and Elite Club, Science and Research Branch, Islamic Azad University, Tehran, Iran

grain boundary doping, and minimization of grain boundary area. Silver nanoparticle inclusion reduces the grain size and increases the strength and hardness of the parent compound. Silver improves not only the critical current density but also magnetic-flux trapping [10, 11]. The controlled addition of Ag in between the grains of YBCO results in better interconnection, which improves weak links and leads to the enhancement in the superconducting properties [12]. Ag addition was reported to be effective in improving the mechanical properties, probably by filling the pores in the grain boundaries. From an application point of view, Ag addition studies on textured Ag-doped superconducting oxides $Y_1Ba_2Cu_3O_{7-\delta}$ (Y-123) improved fracture toughness and the resistance to thermal shock [13]. At mesoscopic level, silver increases plasticity and the resistance to crack formation [14].

This study denotes to the investigation of structural analysis corresponding to different values of $x = 0.00 - 0.6$ wt% Ag nano-sized particles (50 nm) inclusions added to the high-temperature polycrystalline superconductor $Y_1Ba_2Cu_3O_{7-\delta}$ samples which are produced by a conventional solid-state reaction method. Aslamazov–Larkin (AL) theory and Lawrence–Doniach (LD) model were used to determine some discrepancies in pure and doped compounds and also analyze the behavior of thermal fluctuations conductivity above the superconducting transition temperature. Crossover temperature from 2D to 3D (T_{LD}), the zero-temperature coherence length along the c -axis $\xi_c(0)$ and some superconducting parameters such as effective super layer length of the 2D system d were obtained. We calculated interlayer coupling J by two methods (first method (formula) and second method (measured)). We calculated also the anisotropy γ for layered superconducting systems, the thermodynamic critical field $B_c(0)$ at the zero-temperature, the lower critical magnetic field $B_{c1}(0)$, the upper critical magnetic field $B_{c2}(0)$, and the critical current density $J_c(0)$ at the zero temperature.

2 Experimental

Nanosilver powder was prepared from NaBond companies located in Hong Kong, China. The silver nanoparticles have been produced by using laser evaporation process steam. The purity of raw material was 99.5+ % with the average size of 50 nm and spherical morphology shape with white and gray color determined by transmission electron microscopy (TEM). The silver nanoparticles were doped to the YBCO precursor powder by mixing and hand grinding in an agate mortar along with pestle. The doping amount of Ag, in this case, varying from $x = 0$ to $x = 0.6$ wt% of the total mass of the sample. Combined powders were pressed into pellets at 200 bars in the circular disks form

and dimension of 30 mm \times 4 mm. The calcination process involved heating the furnace to 750 °C at the rate of 200 °C/hr and soaking for 12 h, followed by heating to 930 °C at the rate of 150 °C/h and then calcining at 930 °C for 24 h before cooling to room temperature at the rate of 60 °C. The calcined pellets were not of good quality and can be easily broken and divided into layers; therefore, a sintering process was necessary. For the sintering process, the calcined samples were the first ring milled for 20 min, the particles being $< 10 \mu\text{m}$ in size, and the powder was then pressed into pellets using again the 30-mm diameter hardened steel die and uniaxially pressure of 400 bars to obtain approximately a 3-mm thick disk. The pellets were put into the furnace and the temperature increased to 930 °C at the rate of 90 °C per hour. The pellets were sintered at this temperature for 24 h. The temperature was then decreased to 720 °C at a rate of 20 °C per hour, followed by cooling to room temperature in the presence of 1-atmosphere oxygen at the rate of 10 °C per hour. We considered pure powder (0 wt%) as a reference, it was hand ground just as the Ag-doped samples to ensure identical conditions due to physical properties of the samples.

After preparation, the structure and phase identification of YBCO and Ag nanoparticles doping on Y-123 sintered samples were specified by powder X-ray diffraction (XRD) using a Bruker D 8 Advance diffractometer with $\text{CuK}\alpha$ radiation (generator current = 40 mA, generator voltage = 40 mv and $K\alpha = 1.540598\text{\AA}$ in the diffraction angle range of $2\theta = 20^\circ \sim 90^\circ$). Analyzing of X-ray diffraction data was carried out by the Rietveld method and X'Pert high score software. Lattice parameters a , b , and c and the oxygen content are estimated. The morphology and microstructures of specimens were characterized by scanning electron microscope (SEM) using KYKY-EM3200 with accelerating voltage 20 and 26 kV, Resolution 6.0 nm (Tungsten filaments) and magnification $15\times \sim 250000\times$. The samples were sputtered with a thin layer of gold as covering contrast material using SBC-12 ion sputter coater (KYKY Co.).

Resistivity measurements were used to study the normal and superconducting states of the Y-123 materials without applied magnetic fields. The measurements were undertaken using the standard four-point probe method. For determination of T_c via resistivity ρ , after the final heating treatment cycle, the bulk samples are cut into $\sim 20 \times 5.5 \times 2.2 \text{ mm}^3$ sizes carefully. The samples are mounted on a sample holder which is a 16-pin DIL package supplied by SPECTRUM Semiconductor Material, INC. This type of sample holder is very useful as it allows the sample wires to be connected with the aid of a standard binocular microscope. To make sure that there is no electrical contact between the sample and sample holder, a very thin layer of mica, which is a good thermal conductor and electrical

insulator, is used. Thermal paste (zinc oxide) is used to attach the sample to the sample holder. Utilizing the thermal paste reduces the time delay for the thermal equilibrium of the system. Current and voltage wires are connected directly onto the sample surface, or onto evaporated silver pads, using colloidal silver. Contact resistance is estimated to be less than 0.1 ohms. Measurements were performed from 10 to 300 K with an accuracy of 0.1 K while sweeping upward at the rate of 1°C/min.

3 Excess Conductivity Method

The analysis of results for the fluctuation contribution on electrical conductivity is performed by the Aslamazov–Larkin theory which provides the following expression for the excess conductivity above T_c generated by the thermodynamic fluctuations [15]. According to the AL proposal, the fluctuation magneto-conductivity diverges as a power law of the type:

$$\Delta\sigma = A\varepsilon^{-\nu} \quad (1)$$

where A is AL temperature independent constant and ε represents the reduced temperature with the following equation:

$$\varepsilon = (T - T_c^P) / T_c^P \quad (2)$$

where T_c^P is the temperature of the peak obtained from $d\rho/dT$. ν is the Gaussian critical exponent depending on the dimensionality of the high-temperature superconducting system. In the mean-field region and according to the Aslamazov–Larkin (AL) theory [15], the fluctuation induced excess conductivity $\Delta\sigma$ is generally calculated by subtracting the background normal-state conductivity from the measured conductivity as follows [16]:

$$\Delta\sigma = \sigma_m(T) - \sigma_n(T) \quad (3)$$

where $\sigma_m(T)$ is the measured conductivity and $\sigma_n(T)$ is the extrapolated conductivity under the assumption of a linear or a Zou–Anderson dependence for resistivity $\rho(T) = 1/\sigma(T)$ above $2T_c$. Notice that the feature of the normal resistivity as a function of temperature is approximately linear with the following equation:

$$\rho_n(T) = \rho_0 + \beta T \quad (4)$$

and obtained by linear extrapolation of the resistivity data in the high-temperature behavior. Consequently, this permits to perform an easy linear extrapolation to determine σ_n . The dimensionality D of the fluctuation system is related through the expression as follows:

$$\nu = 2 - D/2 \quad (5)$$

The effective value of the critical exponent for 3D and 2D are $\nu = -0.5$ and $\nu = -1$ respectively [17]. The plots of $\ln(\Delta\sigma)$ vs. $\ln(\varepsilon)$ for free and doped Y-123 allow determination of the exponent values from the slopes of linearly fit to correlate the experimental data with theoretically predicted ones. The plots may reveal three distinct regimes, i.e., mean-field region or the Gaussian fluctuations, critical fluctuations, and short-wave fluctuation region.

The values temperature dependent parameter (A) are $A_{3D} = \frac{e^2}{32\hbar\xi_c(0)}$, $A_{2D} = \frac{e^2}{16\hbar d}$, and $A_{1D} = \frac{e^2\xi_c(0)}{32\hbar s}$ which denoted for 3D, 2D, and 1D respectively. $\xi_c(0)$ is the zero temperature coherence length or GL correlation length, “ d ” is the effective separation of CuO₂ layers and s is the wire cross-sectional area of the 1D system, respectively. These relations are based on the GL theory and are valid only for the mean-field temperature region ($1.01T_c$ to $1.1T_c$). Lawrence and Doniach (LD) extended the AL model for layer superconductors, where conduction occurs mainly in 2D CuO₂ planes and these planes are coupled by Josephson tunneling. The excess conductivity parallel to the layers in the LD model is given by the following::

$$\Delta\sigma(T)_{LD} = \frac{e^2}{16\hbar d\varepsilon} \left[1 + \left(\frac{2\xi_c(0)}{d} \right)^2 \varepsilon^{-1} \right]^{-1/2} \quad (6)$$

From this equation at a temperature close to T_c , $2\xi_c(0)/d \gg 1$ and $\Delta\sigma(T)$ diverges as $\varepsilon^{-1/2}$ which corresponds to 3D behavior. Whereas at $T \gg T_c$, $2\xi_c(0)/d \ll 1$ and $\Delta\sigma(T)$ diverges as ε^{-1} which corresponds to 2D behavior. At the transition temperature, T_{2D-3D} , the coherence length along c -axis, $\xi_c(0)$ for polycrystalline samples can be obtained by using the Lawrence-Doniach model as follows [18]:

$$T_{2D-3D} = T_c \left[1 + \left(\frac{2\xi_c(0)}{d} \right)^2 \right] \quad (7)$$

Using this model, the concept of interlayer coupling, J based on Josephson coupling as a result of $\xi_c(0)$ interaction with the superconducting layers is given by the following:

$$J = \left(\frac{2\xi_c(0)}{d} \right)^2 \quad (8)$$

For layered superconducting systems, the anisotropy γ can be written as follows [19]:

$$\gamma = \frac{\xi_{ab}(0)}{\xi_c(0)} \quad (9)$$

where $\xi_{ab}(0)$ is the ab -coherence length which is between 10 and 20Å for copper oxide-based HTSC [18]. The

experimental determination of the Ginzburg number is as follows:

$$N_G = \left| \frac{T_G - T_C}{T_C} \right| = \frac{1}{2} \left(\frac{k_B T_C \gamma}{B_c^2(0) \xi_c^3(0)} \right)^2 = \frac{1}{2} \left(\frac{k_B}{B_c^2(0) \gamma^2 \xi_c^3(0)} \right)^2 \quad (10)$$

where T_C is a critical temperature, T_G is the temperature for finish 3D regime, and k_B is the Boltzmann constant, the thermodynamic critical field $B_c(0)$ is estimated from the relation:

$$B_c(0) = \frac{\varphi_0}{\sqrt{8\pi} \lambda(0) \xi_c(0)} \quad (11)$$

where φ_0 is the flux-quantum number and $\lambda(0)$ the penetration depth. Using the value of $B_c(0)$ and $\lambda(0)$, the lower critical magnetic field $B_{c1}(0)$, upper critical magnetic fields $B_{c2}(0)$, and critical current density $J_c(0)$ are calculated according to the following GL equations:

$$B_{c1} = \frac{B_c \ln k}{\sqrt{2} k} \quad (12)$$

$$B_{c2} = k B_c \sqrt{2} \quad (13)$$

where k is the Ginzburg–Landau parameter and is defined as the ratio of the penetration depth to the coherence length, and finally critical current density is calculated by the following:

$$J_c = \frac{4k B_{c1}}{3 \ln k \sqrt{3} \lambda} \quad (14)$$

4 Results and Discussion

Figure 1 demonstrates the X-ray diffraction patterns of samples for pure YBCO and added with different amounts of Ag nanoparticles doping from 0.06 to 0.6 wt%. In these X-ray diffraction patterns, 19 diffraction peaks are observed at $2\theta = 22.909$ to 87.580 corresponding to the planes of orthorhombic $Y_1Ba_2Cu_3O_{7-\delta}$. All the reflection peaks are indexed with ICSD card [20]. These results indicate that adding a small amount of Ag to the sample has no marked influence on the final product in X-ray resolution. A predominantly single-phase perovskite structure YBCO with orthorhombic Pmmm symmetry and small quantities of secondary phases, such as BaCuO₂ is indicated by data analysis. Apparently, there is no peak corresponding to the Ag-based compounds due to X-ray diffraction patterns.

No impurity up to $x = 0.6$ wt% was considered to be attributed to the reflections, except the Y-123 phase being detected in the X-ray patterns. Figure 1 shows by increasing the Ag nanoparticles, most of the peaks grow and indicating the better crystallization of the grains. This effect is obvious in the peak at 38.633° which is the same result with the

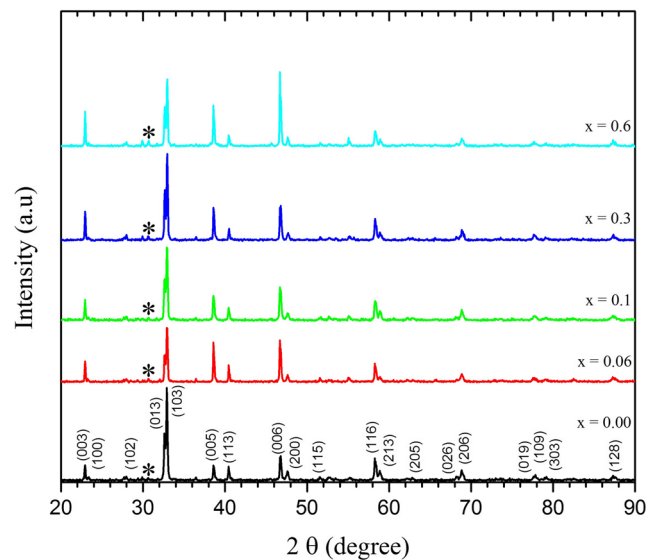


Fig. 1 Powder XRD patterns of the samples for pure YBCO and added Ag nanoparticles doping. Secondary phases are denoted by symbol (*) which is BaCuO₂

ones reported by Farbod et al. [12], and also, at 46.803° particularly with $x = 0.6$ wt%. The lattice parameters a , b , and c for Ag-doping samples which are listed in Table 1 were determined by Rietveld refinements. These data show that the values of lattice parameters a , b , and c for the pure sample are 3.8091, 3.8789, and 11.6435 (Å) respectively. The volume of cell which is equal to abc for all samples (from $x = 0.0$ wt% to $x = 0.6$ wt%) are recorded. The oxygen content is also estimated to be 6.91, 6.86, 6.78, 6.73, and 6.47 for pure and added silver samples related to the $x = 0.0$, $x = 0.06$, $x = 0.1$, $x = 0.3$, and $x = 0.6$ $Y_1Ba_2Cu_3O_{7-\delta} + x$ wt% Ag respectively and are shown in Table 1. Due to this table, increasing of nanoparticle silver doping caused reduction of oxygen content. Superconductivity of YBCO is associated not only with the oxygen content but also with the ordering of the oxygen atoms and oxygen vacancies in the Cu–O basal plane.

According to Fig. 2, although the lattice parameter b remains almost constant the lattice parameters a and c rise with increasing of Ag doping up to 0.3 % and then decrease when the doping reach to the 0.6 %. The trend of change in the lattice parameters a and c with increasing of Ag-doping is the same. These changes may be argued to the substitution of the Cu²⁺ ions which have a small ionic radius (0.058 nm) [21, 22] by the larger Ag²⁺ ions (0.087 nm) [23, 24]. This large ionic radius causes an increase of the lattice parameter c and a while the lattice parameters b remains almost constant (The case of doping 0.6 % is exceptional).

One may note that the average of 0.12 % variation in volume cell which is negligible managed to preserve the orthorhombic crystal structure of the YBa₂Cu₃O₇. In the

Table 1 Lattice structure parameters of YBCO samples with different amounts of Ag nanoparticles doping

	Y-123+ <i>x</i> wt% Ag					
<i>x</i>	0.0	0.06	0.1	0.3	0.6	
<i>a</i> (Å)	3.8091	3.8103	3.8134	3.8193	3.8100	
<i>b</i> (Å)	3.8789	3.8789	3.8784	3.8835	3.8740	
<i>c</i> (Å)	11.6435	11.6287	11.6409	11.6832	11.6300	
Volume of cell(Å ³)	172.03	171.87	172.17	173.29	171.66	
Oxygen content	6.91	6.86	6.78	6.73	6.47	

cause of 0.06 and 0.6 % doping, the volume of the YBCO unit cell and the lattice parameter *c* was decreased with increasing the Ag concentration as indicated in Table 1. The decrease of the *c* parameter may lead to a decrease of the distance between the reservoir planes and in turn enhancing the charge carries transfer into the YBCO orthorhombic crystal. However, The effect of Ag in the Y123 superconductor, researched substitution Ag in the Cu-O chain [25].

Figure 3 indicates that the difference between lattice constants *a* and *b* decreases slightly with the addition of Ag-doping up to 0.1 % which causes the reduction of orthorhombicity $\eta = (b-a)/(b+a)$, with respect to the Ag-free sample that has high value of orthorhombicity similarly is seen with the ones reported by Giri et al. [26]. From 0.1 to 0.6 % Ag-doping, the value of orthorhombicity remains almost constant while oxygen content decreased in all cases.

Figure 4 illustrates the temperature dependence of electrical resistivity for pure YBCO bulk superconductor and Ag nanoparticles doped on YBCO samples. In this figure, the general features of the temperature dependence of the resistivity is the same as the data reported previously [27], which has shown that the high-T_c superconducting samples are generally characterized by a linear temperature

dependence over a large temperature range, unless the stoichiometric composition of the sample differs significantly [28, 29]. Figure 4 indicates the superconducting transition temperature $T_{c \text{ onset}}$, for polycrystalline Y-123 sample, is sharp enough and clear. This value is 93.54 K, 90.93 K, 88.79 K, 84.52 and 74.90 K, from resistivity for samples with Ag nanoparticles addition $x = 0.00$, $x = 0.06$, $x = 0.10$, $x = 0.30$, and $x = 0.60$ respectively. These values decrease significantly when amounts of Ag nanoparticles increase. The $T_{c \text{ onset}}$ depression as seen through the inset of Fig. 4 is more pronounced for Ag added $x = 0.6$ samples. The suppression of $T_{c \text{ onset}}$ is consistent with the known behavior of the bulk superconductors when adding small amounts of magnetic impurities [30–33].

The resistivity curves in the metallic regime can be expressed by the linear equation $\rho_n(T) = \rho_0 + \beta T$, where β is the resistivity temperature coefficient, considered as a parameter that depends on the intrinsic electronic interaction and ρ_0 is the residual resistivity considered as an indicator of the sample homogeneity and defect density. The resistivity of our samples in the normal state is linear (metallic) for pure and those ones with Ag concentration. All of the resistivity is $\leq 2 \times$ larger than for ab-plane resistivity of high purity single crystal Y-123

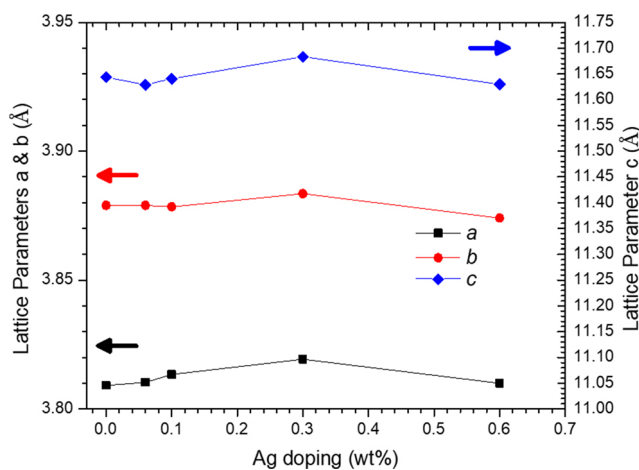


Fig. 2 Variation of lattice parameters *a*, *b*, and *c* for Y-123 samples added with various amounts of nano-sized Ag particles

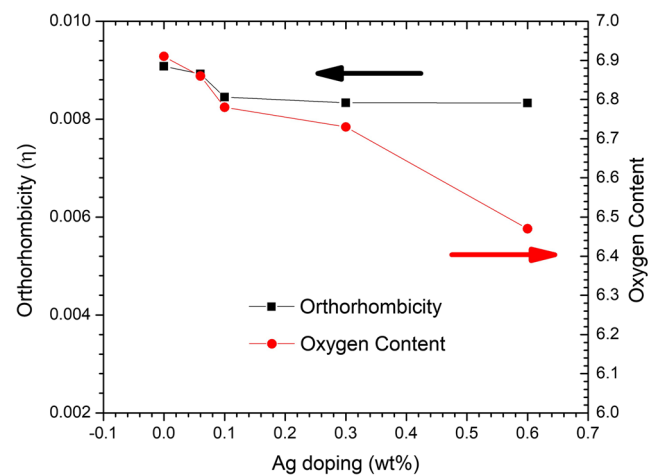


Fig. 3 Variation of orthorhombicity η and oxygen content for Y-123 samples added with various amounts of nano-sized Ag particles

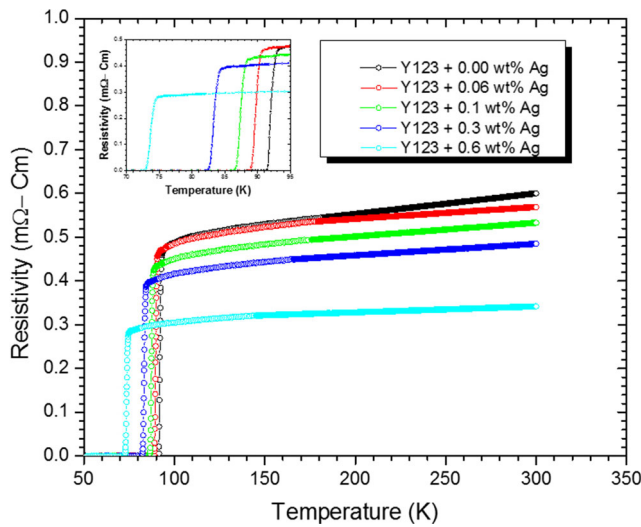


Fig. 4 Resistivity curves versus temperature for the polycrystalline Y-123 samples containing different concentrations of nanoparticle Ag. Inset: the temperature dependence of resistivity for showing exact T_{c0} and T_c

with optimal oxygen content at $T_c = 92$ K [34]. The normal-state resistivity decreases with increasing Ag concentration in all samples. To account for this decrease in resistivity, it is assumed that the dominant process involves decreased electron scattering from both the small and large angle grain boundaries associated with the different crystallographic orientations. The absolute resistivity in the normal state depends on porosity, grain boundary scattering, and its linearity over a longer temperature interval confirms the idea that the preparation and synthesis of the samples are done correctly, i.e., with optimal oxygen content $7 - \delta \leq 6.91$ for pure and Ag-doped YBCO samples.

According to Fig. 4 and its inset can be seen that for all samples, the electrical resistance first decreases linearly with temperature and then begins to decline sharply and reaches zero near T_{c0} , i.e., the electrical resistance for pure sample begins to decline sharply near 92 K and reaches zero near 91 K. Data related to this matter for Y-123+ x wt% Ag concentration is shown in Table 2. These results indicated that the whole of samples would be superconductors under 77.10 K. By increasing samples

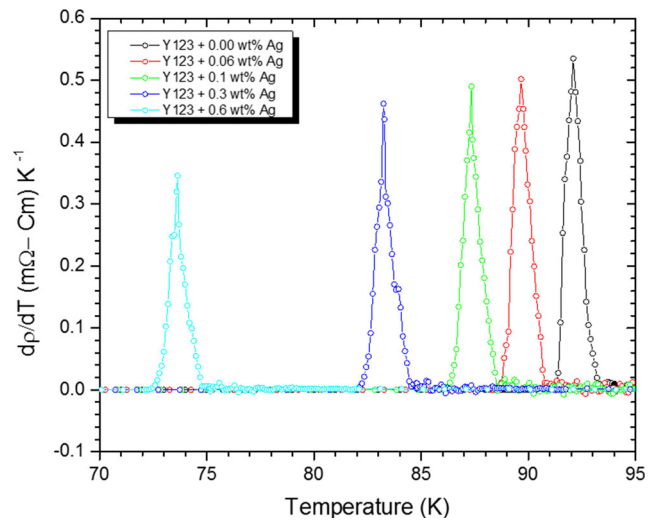


Fig. 5 Plots of $d\rho/dT$ versus temperature of Y-123 samples sintered with different concentrations of nanoparticle Ag

with Ag nanoparticles addition, higher resistivity occurs in normal state. The reason for this can be explained by the disparity in the carrier concentration due to different oxygen doping level and drop off the relaxation time because of a greater number of defects, disorder, and inhomogeneities as the Ag concentration increases.

Figure 5 shows the differentiate of resistivity $d\rho/dT$ curve which is used for determination of the critical superconducting temperature T_c . The temperature corresponding to the maximum of this curve indicates the critical superconducting temperature T_c^P which is shown in Table 2. As Ag nanoparticles content increase the critical temperature (T_c^P) is decreased and suggesting intragranular changes due to the incorporation of silver. The decrease of T_c for Y-123 with 0.6 wt% Ag nanoparticles-doped sample is the largest value in this experiment. Whenever T_c of pure YBCO was reached 92.10 K, it can be compared with the T_c of 0.06 wt% Ag nanoparticles doped sample and abrupt to zero resistivity at the $T_{c\ zero}$ equal to 88.68 K. This experiment indicates that with Ag addition up to 0.6 wt% the T_c of prepared samples will be decreased to 73.65 K eventually as represented in Fig. 4 along with an average of almost 1 K transition widths.

Table 2 Transition temperature, residual resistivity, normal resistivity, and resistivity temperature coefficient associated with resistivity measurement for YBCO samples with different amounts of Ag nanoparticles addition

	Y-123+ x wt% Ag					
x	0.00	0.06	0.1	0.3	0.6	
$T_{c\ onset} (K)$	93.54	90.93	88.79	84.52	74.90	
$T_{c\ zero} (K)$	91.25	88.68	86.06	82.15	72.35	
$T_c^P (K)$	92.1	89.68	87.31	83.26	73.65	
$\rho_0(0K)(m\Omega Cm)$	0.50449	0.49551	0.48399	0.43071	0.31985	
$\rho_n(300K)(m\Omega Cm)$	0.6	0.56901	0.533	0.4848	0.3416	
$\beta = \frac{d\rho}{dT} (\mu\Omega Cm)/K$	0.318352	0.244694	0.164482	0.179775	0.0724095	

In the vicinity of Ag nanoparticles, the T_c values were influenced considerably in all the samples. This scenario has been reported for 0.1 and 0.3 wt% alumina inclusions samples elsewhere [35]. The combination of Al^{3+} ions into the Y site affects the critical temperature T_c of the specimens significantly and degradation of superconductivity will occur consequently [36]. Superconductivity of YBCO is associated not only with the oxygen content but also with the ordering of the oxygen atoms and oxygen vacancies in the Cu-O basal plane. T_c is a sensitive parameter to the electronic structure in the normal state and its large degradation may be attributed to the redistribution of charges in the superconducting system due to the fluctuation of the oxygen ordering caused by a large number of substituted Cu sites. The transition width ΔT_c , was calculated from the $d\rho/dT$ graphs at full width at half maximum of the peaks, is around 0.908 K, 0.999 K, 0.908 K, 0.817 K and 0.818 K for samples with Ag nanoparticles addition $x = 0.00$, $x = 0.06$, $x = 0.10$, $x = 0.30$ and $x = 0.60$ respectively. These data reveal that the samples are in good quality conditions with less than 1 K transition width. However, a broader transition is observed in the case of YBCO samples with $x = 0.06$ Ag addition. The increase of ΔT_c would be affected by percolation paths and the gradual occurrence of a microscopic inhomogeneity with increasing the nanoparticles content. It is eminent that inhomogeneities and characteristics of superconducting grain significantly influence the critical and mean-field regimes and the dimensionality of fluctuation conductivity [31, 37–39].

Transition temperatures related to resistivity measurement, such as $T_{c \text{ onset}}$, $T_{c \text{ zero}}$, T_C^P supplement with residual resistivity ρ_0 , normal resistivity at room temperature ρ_n , and resistivity temperature coefficient β for YBCO samples with different amounts of Ag nanoparticles addition are tabulated in Table 2. By increasing of Ag nanoparticle doping up to $x = 0.6$ wt%, all of the mentioned parameters decreased (β in the $x = 0.3$ wt% case is exceptional). The decrease in T_c can thus be explained as arising due to Ag-induced modification of the grain boundary characteristics and progressively decoupling of the superconducting grains. A grain boundary is a region of structural distortions, where extra energy appears; in order to decrease their energy, they tend to attract impurity atoms. The value of superconducting transition temperatures T_c , for the pure ($x = 0.00$) polycrystalline Y-123 material, determined from the resistivity curve, is significantly higher than those obtained from a different method such as thermoelectric power curves. This result is not unexpected as the two methods used to determine T_c depend on different physical processes. Once there is a sufficient density of Cooper pairs to carry the measurement current in the resistivity determination, the remaining normal electron resistivity is shorted out and T_c

will be obtained. It is well-known that T_c increases with the increase of oxygen due to the broken Cu-O chains in YBCO. T_c increases with the decrease of oxygen in Bi-2212 due to the broken Bi-O chains during post-annealing [40]. The Bi-O chains of Bi-2212 were broken more easily than the Cu-O chains because the bond energy of Bi-O chains is lower than that of Cu-O [41]. Since the resistivities depend on the electron contribution only, and the thermal conductivities may be separated into phonon and electron contributions K_{ph} and K_e an estimate of the upper limit for the electronic contribution to the normal state K^n value can be determined from the Wiedemann–Franz law for sample with oxygen content 6.91 (metallic state) [34].

Figure 6 is depicted to show a graph of $\ln(\Delta\sigma)$ versus $\ln(\varepsilon)$ for free and Ag nanoparticles-doped Y123 samples. This graph is used to compare the experimental data of excess conductivity ($\Delta\sigma$) with the theoretical expression for fluctuation conductivity. For this reason, as shown in Fig. 6a, each plot may be divided into three significant regions namely critical fluctuation, mean-field or Gaussian fluctuations, and short-wave fluctuation regions. Critical fluctuation regime associated with $\nu_{\text{cr}} \approx 0.3$ is depicted in Fig. 6a. This regime was also observed in others not only polycrystalline [30] but also in single crystal [42] and thin film [43] samples. The solid lines in mean-field regions represent theoretical fits with the slopes of -0.5 , -1 and -1.5 for 3-D, 2-D, and 1-D systems, respectively. These three distinct linear parts which indicating fluctuation conductivity behavior in the mean-field region ($-3 < \ln(\varepsilon) < 0$) for each sample are shown in Fig. 6a–e. To compare all the experimental data in one glance Fig. 6f gathered them together.

When the conductivity exponent values are -0.5 , the intercepts of linear fit vary from -2.68446 to -2.27841 , indicating the existence of 3D fluctuations. Then calculated values for A_{3D} leads to the determination of the zero temperature coherence length along the c -axis, $\xi_c(0)$. This parameter varies from 11.144 Å to 7.42496 Å, for the Y-123+ x wt% Ag samples which are listed in Table 3. The shortest $\xi_c(0)$ within the series was 7.42496 Å at $x = 0.6$. Among these values for a pure sample when $x = 0.00$, $\xi_c(0)$ is consistent with the literature for Y123 no added sample. However, by increasing nanoparticle Ag-doped, $\xi_c(0)$ decreased which indicates more disorder state of the samples [3].

When the conductivity exponent values are -1 , the intercepts of linear fit vary from -3.21542 to -2.82565 , representing the existence of 2D fluctuations. Then calculated values for A_{2D} leads to the determination of the super layer length d . This parameter varies from 37.902 Å to 25.6677 Å, for the Y-123+ x wt% Ag ($x = 0.00$ to $x = 0.60$) samples which are named them first method (formula) and the values are recorded in Table 3. The

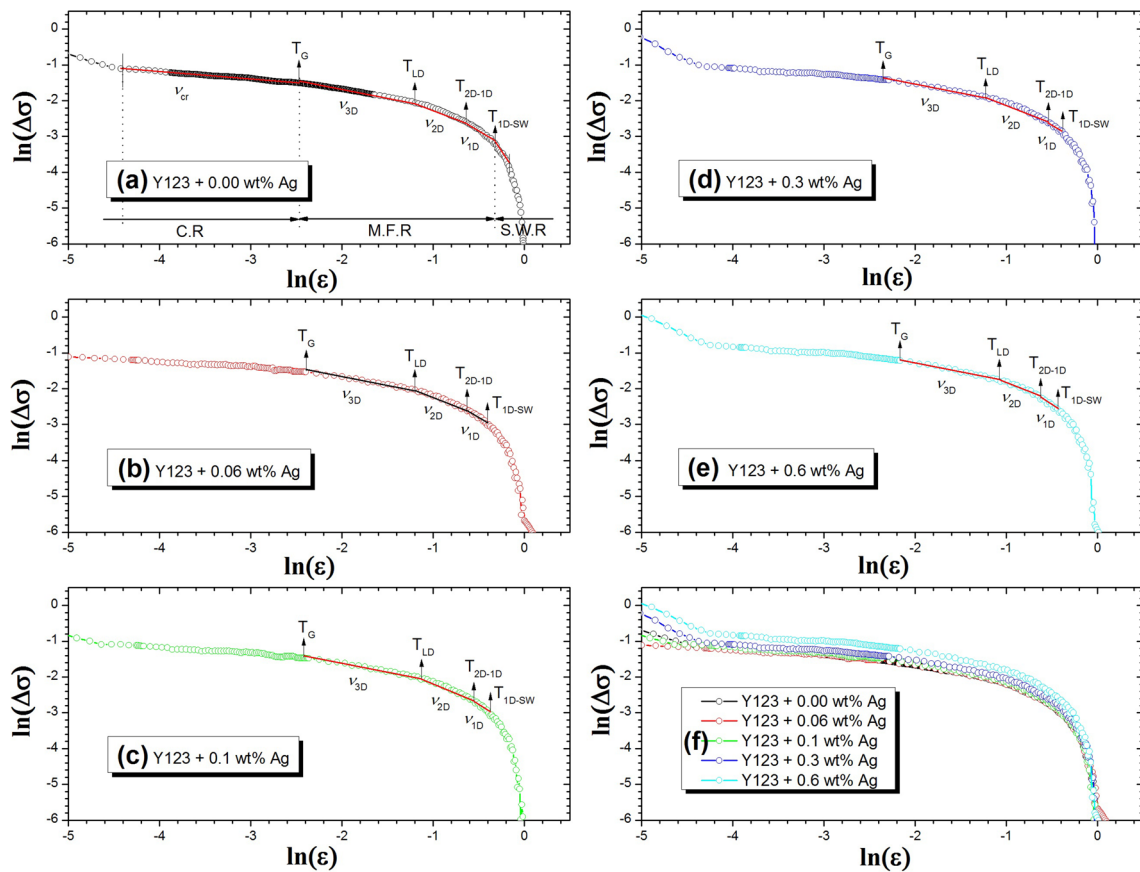


Fig. 6 Plot of $\ln(\Delta\sigma)$ versus $\ln(\epsilon)$ of the Y123+ x wt% Ag nanoparticles doping ($x = 0.00, 0.06, 0.1, 0.3,$ and 0.6) samples. The solid lines represent the theoretical slopes $- 0.5, - 1$ and $- 1.5$ for 3-D, 2-D,

and 1-D systems, respectively. C.R., M.F.R., and S.W.R. are associated with the critical region, mean-field region, and short-wave region, respectively

3D-2D crossover temperatures T_{2D-3D} are calculated from the intersection of the two linear parts and then by substitution of T_{2D-3D} accompany with $\xi_c(0)$ into (7), the

super layer length d is obtained and so-called second method (measured). This parameter (d) varies from 40.4946 Å to 25.2648 Å, for the Y-123+ x wt% Ag samples.

Table 3 Characteristic parameters related to excess conductivity fluctuation analysis for Y-123 samples with different amounts of Ag nanoparticles doping

Y-123+ x wt% Ag	x	0.00	0.06	0.1	0.3	0.6
Intercepts of linear fit for the conductivity	$\nu_{3D} = - 0.5$	- 2.68446	- 2.65988	- 2.61509	- 2.53512	- 2.27841
	$\nu_{2D} = - 1$	- 3.21542	- 3.2036	- 3.16219	- 3.08353	- 2.82565
exponent ν values	$\nu_{1D} = - 1.5$	- 3.59502	- 3.5533	- 3.53803	- 3.43565	- 3.21672
	$\nu_D = - 3$	- 4.22653	-	-	-	-
Coherence length (Å)	$\xi_c(0)$	11.144	10.8734	10.3971	9.59803	7.42496
Super layer	First method (formula)	37.902	37.4567	35.9373	33.2188	25.6677
Length d (Å)	Second method (measured)	40.4946	38.5161	36.3719	35.4	25.2648
Interlayer	First method (formula)	0.34579	0.33708	0.33481	0.33393	0.33471
Coupling J	Second method (measured)	0.30293	0.31879	0.32685	0.29405	0.34547
Anisotropy γ		0.89735	0.91968	0.96181	1.04188	1.34681

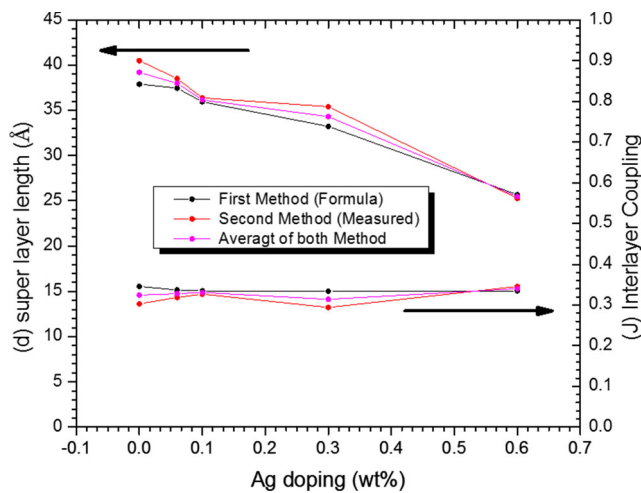


Fig. 7 super layer length d and interlayer coupling J versus different doping for the $Y_{123}+x$ wt% Ag samples by two methods and the average of them

The values of data based on these two methods are very close and to compare them with each other, a graph of the super layer length d versus Ag-doping was plotted accompany with their average in Fig. 7. Inspection of this figure indicates that by increasing nanoparticle silver dopant the super layer length d decreases and anisotropy γ increase (see Table 3). The decrease in super layer length d values implies the unsettling of the mean free path for the charge carriers and an increase in anisotropy γ indicates the number of substitution sites affect the coupling between the CuO₂ planes because the size of the Ag ions, being larger compared to Cu ions and that results in higher anisotropy with addition of silver nanoparticles. Within the framework of AL and LD, the overall interlayer coupling J remain almost constant which indicates that there was no displacement per atom due to the increase of Ag-doping (see Table 3 and Fig. 7).

Different temperatures which are related to their dimensionality fluctuation associated with various Ag nanoparticle content are shown in Table 4. According to this table, lower T_c values than T_{LD} indicates that the thermodynamically activated Cooper pairs are generated within the grain at comparatively higher temperatures but due to the intragranular disturbances the mean-field critical temperature comes down to lower value. It is possible to infer that the 3D Gaussian regime determines the spatial limit for the obtainment of long-range order of the superconductivity in the material bulk [44]. When the temperature is diminished near T_c , first superconductivity is established in the CuO₂ planes, as a 2D regime, and crosses up to a well-defined 3D regime [45].

Scanning electron microscopy (SEM) images with magnification 40000 (a, b, c, d, and e) and 5000 (f, g, h, i, and j) of the pure $Y_1Ba_2Cu_3O_{7-\delta}$ bulk polycrystalline superconductor sample and added ($x = 0.00$, $x = 0.06$, $x = 0.10$, $x = 0.30$, and $x = 0.6$) with nanoparticles Ag inclusions samples are illustrated in Fig. 8. This figure shows that the random orientation of grains and nano-sized silver Ag inclusions consequence a decrease of the grain size in YBCO samples. One can observe that for both sets of images, by increasing the nanoparticles Ag, the homogeneity of the samples and also connectivity between the grains is improved. Lower dimensional effects in the transport properties can occur with the decrease in grain size when the number of grain boundaries increases and consequently imply a greater number of weak links. (see Ref. [11]) [46, 47].

From (11) to (14), the critical magnetic fields, $B_c(0)$, $B_{c1}(0)$, $B_{c2}(0)$, and critical current density $J_c(0)$ for pure and doped samples are determined and presented in Table 5. Compare all the values of $B_c(0)$, $B_{c1}(0)$, $B_{c2}(0)$, and critical current density $J_c(0)$ for free with the doped Y-123 samples, shows by increasing the nanoparticles silver inclusions, the critical magnetic fields and critical current density are enhanced. This scenario indicates the improvement of flux pinning properties.

Table 4 Ag nanoparticle content dependence of different cross over temperatures (Ginzburg–Landau, Lawrence–Doniach, and Shortwave fluctuation) accompany with their temperature range

x	Y-123+ x wt% Ag				
	0.00	0.06	0.1	0.3	0.6
$T_G(K)$	100.03322	98.26901	95.64752	91.24234	82.09421
$T_{LD}(K)$	120	118.26901	115.84752	107.74234	99.09421
$T_{2D-1D}(K)$	142	139.26901	137.84752	130.74234	112.09421
$T_{1D-SWF}(K)$	159	151.26901	146.84752	139.74234	121.09421
ΔT_{v1D}	17	12	9	9	9
ΔT_{v2D}	22	21	22	23	13
ΔT_{v3D}	19.97	20	20.2	16.5	17

Fig. 8 Scanning electron micrographs of $Y_1Ba_2Cu_3O_{(7-\delta)}$ samples prepared via the solid-state reaction method with 0.0 **a, f**, 0.06 **b, g**, 0.1 **c, h**, 0.3 **d, i** and 0.6 wt% **e, j** (magnification 40000 and 5000 respectively) Ag nanoparticles doped. The random orientation of grains and almost modification of grains contact in some sections is evident. Each bar = 1 and 10 μm in magnification 40000 and 5000 respectively

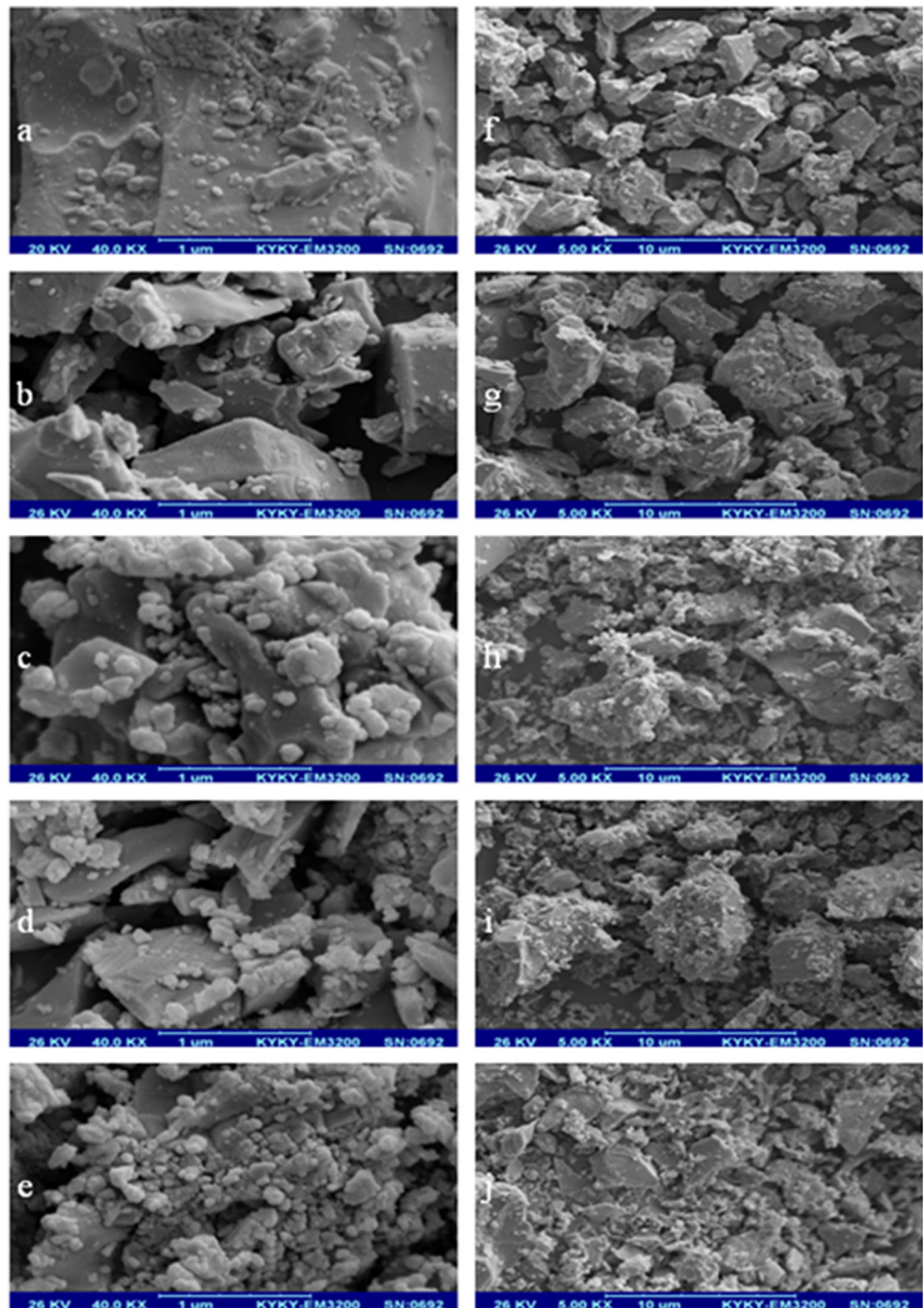


Table 5 Calculated superconducting parameters pure and added Y-123 samples with various amounts of nanoparticles silver inclusions

	Y-123+ x wt% Ag				
x	0.00	0.06	0.1	0.3	0.6
$B_c(0)(T)$	20.88212	21.40176	22.38213	24.24555	31.3415
$B_{c1}(0)(T)$	3.61068	3.65113	3.72483	3.85642	4.27884
$B_{c2}(0)(T)$	265.00248	278.35553	304.44157	357.24405	596.95347
$J_c(0)A/m^2 \times 10^9$	1.13668	1.16496	1.21833	1.31976	1.70602
$J_c(0)A/Cm^2$	113667.83684	116496.41306	121832.90604	131976.05219	170601.50952

5 Conclusion

We have investigated the effect of silver nanoparticle on the conductivity fluctuation and some parameters of high-temperature superconductor polycrystalline YBCO within the framework of AL and LD. Samples were fabricated by the conventional solid-state reaction method by adding Ag up to 0.60 wt%. The electrical resistivity behavior was discussed with respect to the structural and microstructural features. Ag addition demonstrates the effect in suppressing superconductivity, in particular, T_c in all samples. These results could be attributed to the existence of disorder due to a number of substituted Cu sites in YBCO which results in an electronic structure modification of the grains, and as a consequence, the absence of an optimized carrier concentration in the CuO₂ planes. Conclusions show that Ag⁺ ions occupy both Y and Cu (1) sites and with increasing of Ag-doping, orthorhombicity almost will be decreased. Moreover, the inclusion of nanoparticles Ag to the YBCO system brings about structural as well as dimensional changes in the electrical transport properties which can be ascribed to Ag⁺ ions dispersed into the YBCO system and resulting in mesoscopic and microscopic inhomogeneities in the compound. The superconducting and pinning properties are influenced by the level of disorder induced by an increment of nanoparticles Ag inclusions in the YBCO polycrystalline system. By increasing Ag inclusion, T_c and super layer length d decrease while the overall interlayer coupling J remains almost constant and anisotropy γ increase. These results may be due to the redeployment of charges in the superconducting system related to oxygen content, the resistance of the weak link caused by inhomogeneities, lack of displacement per atom, and the number of substitution sites respectively. T_{LD} decreased in the samples with added Ag which indicates the governing nature of fluctuation of cooper pairs in 3D. Variation of lattice parameters and crystallite volume shows the combination of silver into the superconducting grains. Critical magnetic fields $B_{c1}(0)$, $B_{c2}(0)$ and critical current density $J_c(0)$ were indirectly calculated from the Ginzburg–Landau (GL) number and GL equations. By increasing the doping level of silver nanoparticle, these parameters were found to be higher in Ag added YBCO samples compared to the pure Y123, meaning better intrinsic flux pinning properties of doped Y123.

Acknowledgments The results of this article are obtained from the research plan entitled: “Effect of silver nanoparticles doping on critical current density (J_c) and critical temperature (T_c) of high-temperature YBCO superconductor”. Financial grant was supported by the research center, Shiraz Branch, Islamic Azad University, Shiraz, Iran and Iran Nanotechnology Initiative Council (INIC). The authors are grateful to Dr. Ghaffary, Mr. Fatemi, Mr. Nowroozi, and Mrs. Mallahi from Islamic Azad University-Shiraz branch and Mr. Mahmoodinezhad

from the Brandenburg University of Technology, Germany for their help and valuable comments.

References

1. Z. He, T. Habisreuther, G. Bruchlos, D. Litzkendorf, W. Gawalek, *Physica C: Superconductivity* **356**(4), 277 (2001). [https://doi.org/10.1016/S0921-4534\(01\)00282-9](https://doi.org/10.1016/S0921-4534(01)00282-9). <http://www.science/article/pii/S0921453401002829>
2. X. Cui, G. Liu, J. Wang, Z. Huang, Y. Zhao, B. Tao, Y. Li, *Physica C: Superconductivity* **466**(1–2), 1 (2007)
3. Y. Slimani, E. Hannachi, M.B. Salem, A. Hamrita, M.B. Salem, F.B. Azzouz, *J. Supercond. Nov. Magn.* **28**(10), 3001 (2015)
4. N. Strickland, N. Long, E. Talantsev, P. Hoefakker, J. Xia, M. Rupich, T. Kodenkandath, W. Zhang, X. Li, Y. Huang, *Physica C: Superconductivity* **468**(3), 183 (2008). <https://doi.org/10.1016/j.physc.2007.11.013>. <http://linkinghub.elsevier.com/retrieve/pii/S0921453407013858>
5. G. Shams, A. Mahmoodinezhad, M. Ranjbar, *Iranian Journal of Science and Technology, Transactions A: Science* **42**(4), 2337 (December 2018)
6. S. Dadras, Z. Gharehgazloo, *Physica B: Condensed Matter* **492**, 45 (2016)
7. B.A. Malik, M.A. Malik, K. Asokan, *Chinese J. Phys.* **55**(1), 170 (2017). <https://www.sciencedirect.com/science/article/abs/pii/S0577907316301344?via%3Dihub>
8. V. Bartůňek, O. Smrčková, *Ceramics - Silikaty* **54**(2), 133 (2010). http://www.ceramics-silikaty.cz/2010/pdf/2010_02_133.pdf
9. S.N. Abd-Ghani, H.K. Wye, I. Kong, R. Abd-Shukur, W. Kong, In solid state science and technology IV, Advanced materials research, vol. 895 (Trans Tech Publications Ltd), Advanced Materials Research, vol. 895, pp. 105–108. <https://doi.org/10.4028/www.scientific.net/AMR.895.105> (2014)
10. O. Görür, C. Terzioğlu, A. Varilci, M. Altunbaş, *Supercond. Sci. Technol.* **18**(9), 1233 (2005)
11. E. Mendoza, T. Puig, E. Varesi, A. Carrillo, J. Plain, X. Obradors, *Physica C: Superconductivity* **334**(1–2), 7 (2000)
12. M. Farbod, M.R. Batvandi, *Physica C: Superconductivity* **471**(3–4), 112 (2011)
13. P. Diko, G. Fuchs, G. Krabbes, *Physica C: Superconductivity* **363**(1), 60 (2001)
14. J. Joo, J. Kim, W. Nah, *Supercond. Sci. Technol.* **11**(7), 645 (1998)
15. L. Aslamazov, A. Larkin, In 30 Years Of The Landau Institute—Selected Papers (World Scientific, 1996), pp. 23–28
16. P. Pureur, R.M. Costa, JrP. Rodrigues, J. Kunzler, J. Schaf, L. Ghivelder, J. Campá, I. Rasines, *Physica C: Superconductivity* **235**, 1939 (1994)
17. X. Tang, Q. Liu, J. Wang, H. Chan, *Appl. Phys. A* **96**(4), 945 (2009)
18. A.A. Yusuf, A. Yahya, N.A. Khan, F.M. Salleh, E. Marsom, N. Huda, *Physica C: Superconductivity* **471**(11–12), 363 (2011)
19. N.A. Khan, N. Hassan, M. Irfan, T. Firdous, *Physica B: Condens. Matter* **405**(6), 1541 (2010)
20. M. Francois, A. Junod, K. Yvon, A. Hewat, J. Capponi, P. Strobel, M. Marezio, P. Fischer, *Solid State Commun.* **66**(10), 1117 (1988)
21. M. Hafez, F. Al-Marzouki, W.E. Mahmoud, *Mater. Lett.* **65**(12), 1868 (2011)
22. F.A. Al-Agel, E. Al-Arfaj, A.A. Al-Ghamdi, B.D. Stein, Y. Losovyj, L.M. Bronstein, F. Shokr, W.E. Mahmoud, *Ceram. Int.* **41**(1), 1115 (2015)
23. H.S. Al-Ghamdi, W.E. Mahmoud, *J. Lumin.* **145**, 880 (2014)
24. H.S. Al-Ghamdi, W.E. Mahmoud, *Mater. Lett.* **105**, 62 (2013)

25. D. Cahen, Z. Moisi, M. Schwartz, *Mater. Res. Bull.* **22**(11), 1581 (1987)
26. R. Giri, V. Awana, H. Singh, R. Tiwari, O. Srivastava, A. Gupta, B. Kumaraswamy, H. Kishan, *Physica C: Superconductivity and its applications* **419**(3-4), 101 (2005)
27. M. Gurvitch, A. Fiory, *Phys. Rev. Lett.* **59**(12), 1337 (1987)
28. C. Varma, P. Littlewood, S. Schmitt-Rink, E. Abrahams, A. Ruckenstein, *Phys. Rev. Lett.* **63**(18), 1996 (1989)
29. J. Phillips, *Phys. Rev. B* **40**(10), 7348 (1989)
30. M. Sahoo, D. Behera, *J. Mater. Sci. Eng.* **1**(115) (2012)
31. I. Bouchoucha, F.B. Azzouz, M.B. Salem, *J. Supercond. Nov. Magn.* **24**(1-2), 345 (2011)
32. Y. Xu, M. Izumi, Y. Zhang, Y. Kimura, *Physica C: Superconductivity* **469**(15-20), 1215 (2009)
33. Y. Xu, M. Izumi, K. Tsuzuki, Y. Zhang, C. Xu, M. Murakami, N. Sakai, I. Hirabayashi, *Supercond. Sci. Technol.* **22**(9), 095009 (2009)
34. G. Shams, J. Cochrane, G. Russell, *Physica C: Superconductivity* **363**(4), 243 (2001)
35. V. Antal, M. Kaňuchová, M. Šefčíková, J. Kováč, P. Diko, M. Eisterer, N. Hörhager, M. Zehetmayer, H. Weber, X. Chaud, *Supercond. Sci. Technol.* **22**(10), 105001 (2009)
36. M.S.M. Suan, M.R. Johan, *Physica C: Superconductivity* **492**, 49 (2013). <https://doi.org/10.1016/j.physc.2013.05.022>. <http://linkinghub.elsevier.com/retrieve/pii/S0921453413003067>
37. E. Hannachi, Y. Slimani, M.B. Salem, A. Hamrita, D. Mani, M.B. Salem, F.B. Azzouz, *Mater. Chem. Phys.* **159**, 185 (2015)
38. A.A. Aly, N. Mohammed, R. Awad, H. Motaweh, D.E.S. Bakeer, *J. Supercond. Nov. Magn.* **25**(7), 2281 (2012)
39. A. Mohanta, D. Behera, *Physica C: Superconductivity* **470**(4), 295 (2010)
40. Q. Hao, C. Li, S. Zhang, J. Feng, M. Du, *Physica C: Superconductivity and its applications* **471**(21-22), 1100 (2011)
41. P.K. Gallagher, H.M. O'Bryan, S. Sunshine, D. Murphy, *Mater. Res. Bull.* **22**(7), 995 (1987)
42. J.R. Rojas, A. Jurelo, R.M. Costa, L.M. Ferreira, P. Pureur, M. Orlando, P. Prieto, G. Nieva, *Physica C: superconductivity* **341**, 1911 (2000)
43. P. Mayorga, D. Téllez, Q. Madueno, J. Alfonso, J. Roa-Rojas, *Braz. J. Phys.* **36**(3B), 1084 (2006)
44. J. Roa-Rojas, D. Téllez, M. Rojas Sarmiento, *Braz. J. Phys.* **36**(3B), 1105 (2006)
45. A. Kujur, D. Behera, *Thin solid films* **520**(6), 2195 (2012)
46. S. Falahati, F. Saeb, V. Daadmehr, *Iranian Journal of Physics Research* **9**(1), 43 (2009)
47. X. Wang, J. Horvat, G. Gu, K. Uprety, H. Liu, S. Dou, *Physica C: Superconductivity* **337**(1-4), 221 (2000)

Publisher's Note Springer Nature remains neutral with regard to jurisdictional claims in published maps and institutional affiliations.